

PCCP

Accepted Manuscript



This is an *Accepted Manuscript*, which has been through the Royal Society of Chemistry peer review process and has been accepted for publication.

Accepted Manuscripts are published online shortly after acceptance, before technical editing, formatting and proof reading. Using this free service, authors can make their results available to the community, in citable form, before we publish the edited article. We will replace this *Accepted Manuscript* with the edited and formatted *Advance Article* as soon as it is available.

You can find more information about *Accepted Manuscripts* in the [Information for Authors](#).

Please note that technical editing may introduce minor changes to the text and/or graphics, which may alter content. The journal's standard [Terms & Conditions](#) and the [Ethical guidelines](#) still apply. In no event shall the Royal Society of Chemistry be held responsible for any errors or omissions in this *Accepted Manuscript* or any consequences arising from the use of any information it contains.

Electronically Excited States of Cob(II)alamin: Insights from CASSCF/XMCQDPT2 and TD-DFT Calculations

Brady D. Garabato,^a Neeraj Kumar,^a Piotr Lodowski,^b Maria Jaworska^b and
Pawel M. Kozlowski,^{a,c,†}

^a Department of Chemistry, University of Louisville, Louisville, Kentucky 40292, United States

^b Department of Theoretical Chemistry, Institute of Chemistry, University of Silesia,
Szkolna 9, PL-40 006 Katowice, Poland

^c Visiting professor at Department of Food Sciences, Medical University of Gdansk, Al. Gen. J. Hallera 107, 80-416
Gdansk, Poland

†Correspondence:
Prof. Dr. Pawel M. Kozlowski
University of Louisville
Department of Chemistry
2320 South Brook Street
Louisville, KY 40292, USA
pawel@louisville.edu

Introduction

The reduced form of vitamin B₁₂ (cob(II)alamin or B_{12r}, Figure 1), where the cobalt metal has an oxidation state of +2, is typically generated after homolytic cleavage of the Co-C bond, and is found in many areas of B₁₂ chemistry and biochemistry.^{1,2,3} Cob(II)alamin is a five-coordinate radical complex where the Co^{II}(d⁷) ion is equatorially ligated by four nitrogen atoms of the corrin macrocycle, and axially, by dimethylbenzimidazole (DBI), which may be replaced by a histidine residue, or water, depending on environmental conditions. Due to the axially symmetric g-tensor of the paramagnetic Co^{II}(d⁷) center, electron paramagnetic resonance (EPR) spectroscopy has been a very sensitive probe of the local environment of cobalt.^{4,5,6,7,8,9,10,11,12,13}

Analogs of cob(II)alamin can be found both in solution, and in enzymatic environments at physiological pH. Under non-enzymatic conditions, cob(II)alamin may be generated by the one-electron reduction of Co(III)-based cobalamins (such as aquacobalamin) electrochemically, or chemically by using an appropriate reductant.^{13,14} Upon reduction, the resulting Co(II)-based species forms a stable five-coordinate low-spin radical complex, where the unpaired electron resides entirely on the Co d_{z²} orbital.⁵ Cob(II)alamin has been characterized by x-ray,¹⁵ and the structural features of the Co(II)-corrin moiety are similar to the biologically active forms of vitamin B₁₂ (i.e., the Co(III)-corrins), with the exception of axial Co(II)-N_{DBI} distances are generally shorter.

Cob(II)alamin appears in adenosylcobalamin (AdoCbl)-dependent enzymatic reactions where substrate binding initiates homolytic cleavage of the Co-C bond. The kinetics of Co-C cleavage in (AdoCbl)-dependent enzymes, such as methylmalonyl-CoA mutase, glutamate mutase and ethanolamine ammonia-lyase, have been studied using stopped-flow methods, by detecting visible absorption changes associated with the adenosylcob(III)alamin ($\lambda_{\text{max}} \sim 525$ nm), and cob(II)alamin ($\lambda_{\text{max}} \sim 470$ nm) transitions.^{16,17,18,19,20} The formation of Co(II)-based intermediates, and their interactions with substrate radicals have been extensively investigated by EPR spectroscopy to characterize radical centers inside enzymatic environments.²¹

In methylcobalamin (MeCbl)-dependent methyltransferases, heterolytic cleavage of the Co(III)-C bond leads to the formation of cob(I)alamin intermediates.^{22,23} The highly reactive cob(I)alamin is occasionally oxidized to the undesired cob(II)alamin byproduct, and requires reactivation. It has been suggested that this reactivation step involves an axial ligand switch of the upper ligand to water, to form a five-coordinate cob(II)alamin complex,^{14,24} and a recent theoretical study predicted that the reactivation mechanism involves reorientation of the water ligand, and formation of a Co(I)-H bond.^{25,26} The reduction of cob(II)alamin to the cob(I)alamin intermediate species also takes place in ATP corrinoid adenosyltransferases such as CobA, PduO, and EutT, in which reorientation of the water ligand may also occur.^{27,28,29,30}

Cob(II)alamin may alternatively be generated by photolytic cleavage of the Co-C bond in alkyl cob(III)alamins.^{31,32,33,34,35,36,37,38,39,40,41,42,43} The specific mechanism of the Co-C bond photo-homolysis depends on a number of factors, such as the nature of the upper axial ligand, either the base-on or base-off form, and the excitation wavelength. Based on time-resolved spectroscopic measurements of it is apparent that the Co(II)-based intermediates are inherent part of cob(III)alamins photochemistry and may be referred to as either an electronically excited state, or the ground state of cob(II)alamin.

Despite the importance of the Co(II)-based intermediates in B₁₂ chemistry, a detailed understanding of their electronic properties, and low-lying excited states remains limited. Analysis of electronic excitations is thus required to develop a detailed understanding of the photochemical reactions of the alkylcobalamins, such as MeCbl, and AdoCbl. Typically, time-dependent

density functional theory (TD-DFT) is the only viable method employed to study the excited states of these complex systems. However, the question that commonly arises with TD-DFT applied to large systems, is how appropriate are the descriptions of the excited states. One of the main objectives of this study therefore, is to provide insight regarding the low-lying excited state electronic properties of four- and five-coordinated cob(II)alamins at the TD-DFT level, and by employing wavefunction-based methods. This study may be thus summarized in three parts: (i) investigation of low-lying electronically excited states using CASSCF calculations followed by multi-configurational second-order perturbation theory (XMCQDPT2) to establish a benchmark, (ii) analysis of Configuration State Functions (CSFs) to validate electronic excitations calculated at the TD-DFT level, and (iii) evaluation of the dependency of low-lying excited state manifolds on Co-N axial distance, where elongation of the cob(II)alamin axial bond leads to formation of the base-off form.

2. Computational details

2.1. Structural Models

The full structure of cob(II)alamin (Figure 1, upper panel) may either be obtained either from existing crystal structure,¹⁵ or derived from other high resolution alkylcobalamin crystals,^{44,45} by removing the corresponding upper ligand.⁴⁶ It has been shown that electronic structures produced by both methods are not affected by the initial geometry, whereas their optimizations are sensitive to choice of functional. In this work the later strategy was used, and the full cob(II)alamin structural model was adopted from recent EPR study.⁴⁶ The geometry was obtained by optimization of a modified MeCbl high resolution crystal structure at the BP86/TZ2P level of theory,^{47,48,49} with relativistic corrections included in the optimization step using the scalar-relativistic zeroth-order-regular-approximation Hamiltonian (SC-ZORA),⁵⁰ implemented in the Amsterdam Density Functional (ADF) program.⁵¹

To reduce computational costs, the full cob(II)alamin structure was truncated with respect to side-chains by replacing them with H-atoms, the dimethylbenzimidazole (DBI) base was replaced with imidazole (Im), and the nucleotide loop was removed (Figure1, lower panel). The truncated model, denoted Im-[Co^{II}(corrin)]⁺, has an overall charge of +1 due to the lack of the nucleotide PO₄⁻ group. Additionally, a model with no axial ligand was constructed from the five-coordinate structure by removing its axial base, and is denoted [Co^{II}(corrin)]⁺. Although the PO₄⁻ group is not included in the truncated structural model, this modification does not significantly alter the character of the low-lying excited state manifold, mainly due to the corresponding cobalamin excitations being localized within the corrin ring. Likewise, the removal of the PO₄⁻ group also does not have a significant effect on electronic structure, as may be verified by retention of state order, and character between the truncated, and cob(II)alamin models when comparing their frontier MOs at the same level of theory.

2.2 DFT and TD-DFT Calculations

DFT and TD-DFT calculations performed in this study were carried out using either the TURBOMOLE⁵² and Gaussian09⁵³ suites of programs for electronic structure calculations. In all calculations, the low-spin doublet state ($S = \frac{1}{2}$) of the Co(II) species was assumed. Vertical electronic excitations for the full structure of cob(II)alamin, and the truncated models, along with corresponding Natural Transition Orbitals (NTOs)⁵⁴ were obtained at the TD-DFT level using the BP86 functional, and the 6-311G(d,p) basis set, or Stuttgart-Dresden (SDD) pseudopotential basis sets using the Gaussian09 program. The Stuttgart-Dresden potentials used to include scalar relativistic effects were DF-relativistic 10-electron effective core potential (MDF10

ECP) for Co, quasi-relativistic 2-electron ECP (MWB2 ECP) for C, N, O and P, and the 1-electron ECP (D95 ECP) for H as implemented in Gaussian09. The SDD basis sets were employed mainly to make calculations for the full cob(II)alamin model tractable. Throughout this work, individual molecular orbitals (MOs) compose TD-DFT transitions, while NTOs, which may be composed of multiple donor or acceptor MOs, are referred to as NTO holes and particles, or an NTO hole-particle pair, referring to the contribution to the transition. To obtain the potential energy surface (PES) of the ground state, and lowest excited states for the five-coordinate model, the Co-N_{im} bond was systematically changed and fixed while all other coordinates were optimized at each point, using a step size of 0.05 Å, from 1.80-2.80 Å. TD-DFT vertical excitations along Co-N_{im} coordinate were calculated at the UBP86/6-311G(d,p) level of theory. DFT geometry optimization of the truncated model of cob(II)alamin was also performed using the TURBOMOLE package at the UBP86/TZVPP level of theory. For the full structure, TD-DFT vertical states were calculated at the UBP86/SDD level of theory using the optimized geometry at the UBP86/6-311G(d,p) level of cob(II)alamin to extend the range of calculated excited states at reduced computational cost.

2.3. CASSCF/XMCQDPT2

The electronic properties and low-lying excited states of four-, and five-coordinate model complexes of cob(II)alamins (Figure 1, lower panel), were initially investigated by complete active space self-consistent field (CASSCF) calculations for benchmarking purposes, using the Firefly quantum chemistry package, version 8.0.0.⁵⁵ However, CASSCF calculations alone are not sufficiently accurate, and need to be corrected by second order perturbation theory to account for dynamic correlation. Subsequently, a modified version of multi-configurational quasi-degenerate second order perturbation theory, referred to as XMCQDPT2,⁵⁶ was applied to include the dynamic correlation effects in CASSCF calculations at the perturbation level. Note that, the XMCQDPT2 approach is a genuine multi-root (i.e., perturb-then-diagonalize) multi-reference perturbation theory technique using the CASSCF state-averaged (SA) electron density over the ground and excited states of interest, allowing a true mixing of the CASSCF zeroth-order states via the construction, and subsequent diagonalization of the effective Hamiltonian.⁵⁷ To obtain accurate results, excited-states based on CASSCF/XMCQDPT2 calculations require the determination of a manifold of electronically excited states for analysis of low-lying states of interest, and they are particularly important for transition-metal systems like cobalt corrinoids, where several low-lying electronic states may interact one with another. Twenty electronic states were considered in state average (SA-CASSCF) calculations using 11 electrons and 12 orbitals in the active space. Details regarding the selection of active orbitals used in CASSCF/XMCQDPT2 calculations reported in this work are discussed in Sections 3.1. CASSCF/XMCQDPT2 calculations were performed using the 6-31G(d) basis set, at the optimized geometries of [Co^{II}(corrin)]⁺, and Im-[Co^{II}(corrin)]⁺ as previously mentioned.

3. Results and discussion

To begin, we discuss the electronic structure and low-lying excited states of the four-coordinate cob(II)alamin model, followed by analysis of the five-coordinate model for comparison. Electronically excited states of the truncated models produced by CASSCF/XMCQDPT2 are discussed first, followed by comparison of the corresponding TD-DFT states. The full cob(II)alamin structure at the TD-DFT level is then considered to analyze the influence of corrin side chains on the low-lying excited states, and to make further comparison with experimental spectra. Finally, the influence of Co-N_{im} axial distance on the low-lying excited states is discussed to determine how the electronic properties of cob(II)alamins are modulated by lower axial ligands.

3.1. Four-coordinate model of cob(II)alamin

Analysis of the low-lying excited state manifold for the four-coordinated model (Figure 1) begins by first considering excitation energies calculated by state average (SA) multiconfigurational SA-CASSCF calculations, followed by analysis of configuration state function (CSF) composition at the perturbation level. CASSCF and CASSCF-based multireference calculations such as the XMCQDPT2 approach however, are challenging when applied to large molecules containing transition metals coordinated by aromatic systems, and results obtained strongly depend on the choice of the active space. In the case of the CASSCF calculations for $[\text{Co}^{\text{II}}(\text{corrin})]$, the selection of active orbitals was guided by active spaces previously used for various derivatives of vitamin B₁₂.^{58,59,60,61,62,63,64} The cob(II)alamin intermediate is among a class of Co^{II} square-planar complexes, where the local environment of cobalt in $[\text{Co}^{\text{II}}(\text{corrin})]$ causes splitting of d orbitals, with d^7 as the dominant electronic configuration. Therefore, all five d orbitals are equally important for CASSCF calculations to investigate electronic properties. For such systems, the proper active space, therefore requires the inclusion of cobalt d orbitals, π orbitals of corrin as well as σ orbitals associated with axial bonding. Several other compositions have been previously tested, leading to the most appropriate choice of active space based on the distribution of 11 electrons between 12 active orbitals. Five d Co orbitals and one π occupied corrin MO were combined with their corresponding virtual orbitals, as shown in Figure 2. To account for the double shell effect in transition metal complexes, 4d correlating orbitals are added to the doubly occupied 3d. The occupied π corrin orbitals are correlated with the unoccupied π^* orbitals in the active space.

SA-CASSCF was used to compute 20 electronic states, followed by second order perturbation theory calculations based on the quasi-degenerate approach by Nakano (QDPT2), and its modification by Granovsky, (XMCQDPT2), which uses the CASSCF reference wavefunction to include dynamic correlation. Similar to previous studies of B₁₂ derivatives, a large number of $[\text{Co}^{\text{II}}(\text{corrin})]^+$ excited states at the CASSCF level were considered to allow for intrinsic mixing at the correlated level (XMCQDPT2), and to improve the zeroth-order description of first five states of $[\text{Co}^{\text{II}}(\text{corrin})]^+$. The resulting excitation energies and their compositions in terms of CASSCF configurations are listed in Table 1. Inclusion of dynamic correlation reveals that the D_0 and D_1 states corrected by XMCQDPT2 are a mixture of the first two CAS states. The first, and second CAS states have wavefunctions with one major CSF, with weight percentages of 94% and 85%, respectively. This CSF corresponds to two electronic configurations, $(d_z^2)^1$, and $(d_{yz})^1(d_z^2)^2$. The first has a larger weight contribution to D_0 state, while the second has a larger contribution to D_1 , as shown in Table 1. Considering the compositions of the CAS states involved in the D_0 and D_1 XMCQDPT2 states, we may conclude that in D_0 , the unpaired electron is mainly localized on d_z^2 orbital, while in D_1 it is mainly localized on d_{yz} (with some admixture of $(d_{yz})^1$ occupation in D_0 , and $(d_z^2)^1$ in D_1). This can be considered an inversion of population, revealing that the D_1 excited state is almost degenerate with respect to the D_0 ground state, with very low excitation energy (0.01 eV).

The next three electronically excited states of $[\text{Co}^{\text{II}}(\text{corrin})]^+$ model complex predicted at the XMCQDPT2 level do not mix CASSCF states. These excited states involve more than one dominant configuration in their wavefunction, and are mainly characterized as d-d type electronic transitions involving excitations to the d_{z^2} orbital. In particular, the D_2 has a dominant CSF of 68% $(d_{x^2-y^2})^1(d_z^2)^2$ with a 15% contribution from a $(d_{xz})^1(d_{yz})^1(d_z^2)^2(d_{xy}-n)^1$ doubly excited configuration, and can be characterized as a $d_{x^2-y^2} \rightarrow d_z^2$ transition. D_3 is mainly composed of two $(d_{x^2-y^2})^1(d_{yz})^1(d_z^2)^2(d_{xy}-n)^1$ doubly excited configurations, having 35% and 26% weight contributions to the transition, while the remaining two $(d_{xz})^1(d_z^2)^2(d_{xy}-n)^1$ configurations with 18%

and 11% weight contributions are also symmetric, and characterized as $d_{xz} \rightarrow d_{xy-n}$ transitions. D_3 is thus characterized as a $d_x^2 - y^2/d_{xz} \rightarrow d_z^2/d_{xy-n}$ transition, with a small contribution, coming from a $d_{xz} \rightarrow d_{xy-n}$ excitation. The D_4 excited state has two dominant CSFs which are also composed of two $(d_{xz})^1(d_{yz})^1(d_z^2)^2(d_{xy-n})^1$ doubly excited configurations, with 62% and 26% weight contributions, similarly characterized as a $d_{xz}/d_{yz} \rightarrow d_z^2/d_{xy-n}$ transition. Due to the involvement of doubly excited configurations in the four-coordinate multiconfigurational model, D_3 and D_4 cannot be directly compared to TD-DFT.

TD-DFT calculations based on UBP86/6-311G(d,p) were then applied to analyze and compare excited states obtained from *ab initio* calculations. The Kohn-Sham frontier α and β orbitals for $[\text{Co}^{\text{II}}(\text{corrin})]^+$ model complex obtained from UDFT calculations, along with orbital energies are shown in Figure S1, (Supporting Information), and corresponding TD-DFT excitation energies, and transition characters of the 10 lowest excited states in Table S1. The selected orbitals shown in Figure S1 are relevant to low-lying excitations, and range from H-4 to L+2 for the α , and H-4 to L+3 for the β subspaces.

DFT calculations based on BP86/6-311G(d,p) indicate that the highest occupied molecular orbitals (HOMOs) are a mixture of Co d and π orbitals of the corrin macrocycle. One apparent difference between the DFT frontier orbitals and natural orbitals selected for SA-CASSCF, is mixing of DFT π MOs with the 3d orbitals. It may be noticed, that the unpaired electron of $[\text{Co}^{\text{II}}(\text{corrin})]^+$ is located on H-4(α ,91), which is characterized as a $d_z^2 + \pi$ orbital, and the corresponding unoccupied β orbital, L(β ,95) is the lowest unoccupied MO (LUMO), and characterized as a pure d_z^2 type orbital.

To investigate the energetics and composition of the excited states of $[\text{Co}^{\text{II}}(\text{corrin})]^+$ determined by TD-DFT methods, analysis of electronic transitions based on NTOs was also performed. NTOs of the four-coordinate $[\text{Co}^{\text{II}}(\text{corrin})]^+$ based on TD-DFT calculations, are presented in Figure 3. The lowest excited state determined by UBP86/6-311G(d,p) were characterized as an excitation from a mixed $d_{yz} + \pi$ orbital, where the involvement of π is small with the unoccupied d_z^2 orbital, and is mainly characterized d-d type transitions. The same character is noticed in the D_2 state, but in this case, the transition is $d_{xz} \rightarrow d_z^2$. These states are characterized by low excitation energies close to each other, equal to 0.45 eV and 0.68 eV, respectively. The D_3 state is also of d-d type from a $d_x^2 - y^2 \rightarrow d_z^2$ excitation with a transition energy of 1.38 eV. Consistent with SA-CASSCF, the lowest three excited states are d-d type with excitations to the d_z^2 orbital. The next two states, D_4 and D_5 , can be characterized as mainly $\pi \rightarrow d_z^2$ excitations, with mixed $d\pi \rightarrow \pi^*$ transitions.

The first excited states are of d-d type, similar to XMCQDPT2 calculations, and the ground state is composed of a d_z^2 configuration. We may note the difference in energy of the first excited state, which is 0.45 eV higher than the ground state for TD-DFT, but is nearly degenerate in XMCQDPT2 calculations. The main difference between electronic structures determined by *ab initio*, CASSCF/XMCQDPT2, and DFT calculations, is that there is no degeneracy between the ground and first excited state for DFT, although the first transition is similarly $d_{yz} \rightarrow d_z^2$. We observe qualitative agreement in the characters of the first excited state, although there is some difference in energy. The energy and character of the D_2 state determined by CAS, and the D_3 state determined by TD-DFT, are in a good agreement. The D_2 TD-DFT state in fact has no counterpart in XMCQDPT2 calculations, and is of $d_{xz} \rightarrow d_z^2$ character with some π orbital mixture. It is important to mention the involvement of such configurations relevant to transitions in the D_3 state obtained by XMCQDPT2 calculations (Table 1), but this state is much higher in energy (2.05 eV) and electronic transition involving also $d_x^2 - y^2$ occupied and d_{xy-n} unoccupied molecular orbitals. We also note correlation between TD-DFT and CASSCF calculations, in that the lowest states are d-d type, and that the first excited state is very low in energy.

As shown in Figure 3, the lowest five TD-DFT excited states correspond almost exclusively to the β subspace, where the first four excited states are transitions on d_z^2 orbital. Furthermore, negligible α contributions to each TD-DFT excited state may also be attributed to π MO mixing. TD-DFT calculations also show near degeneracy between the first (0.45 eV) and second (0.68 eV) excited states. D_1 and D_2 states are very close to each other in energy, and are both transitions to the d_z^2 orbital from d-orbitals of cobalt. It may be noted that the D_1 state calculated by TD-DFT is composed an α d_z^2 orbital that does not participate to any significant extent in the transition (Figure 3), but may be interpreted as (TD-DFT) ground state character. The D_1 electronic state is thus characterized by an $(d_{yz})^1(d_z^2)^2$ configuration with some participation of the $(d_x^2)^1$ configuration of the D_0 ground state. Taking into account that the two first states from SA-CASSCF/XMCQDPT2 calculations are nearly degenerate with inverted weight contributions from $(d_z^2)^1$ and $(d_{yz})^1(d_z^2)^2$ electronic configurations, the D_1 electronic state from TD-DFT calculations correlates to the D_1 /XMCQDPT2 excited state. This characteristic of the ground state in the four-coordinate model, is also consistent with the five-coordinate ligand field (LF) state, as will be discussed further in the section regarding axial base dependence, and may be immediately observed in the five-coordinate minima as a significant contribution to D_1 from the α subspace. It should also be noted that the transition dipole moments of the lowest excited states of $[\text{Co}^{\text{II}}(\text{corrin})]^+$ calculated by both SA-CASSCF and TD-DFT are consistent with each other, and are both very low. As expected, the energy of the D_1 excited state calculated by TD-DFT is comparably greater than that by SA-CASSCF, by 0.44 eV. In contrast, the energy of the D_2 excited state computed by TD-DFT is lower by 0.67 eV, than that determined by SA-CASSCF. Similarly, D_3 and D_4 by TD-DFT are 0.67 eV lower, and 0.66 eV lower, respectively, than by SA-CASSCF.

3.2 Five-coordinate model of cob(II)alamin

Having determined the electronic structure and composition of the low-lying excited states of the four-coordinate model, we then consider a more realistic model containing imidazole as the axial ligand, as typically found in biological systems containing derivatives of B_{12} . Similar to the four-coordinate model, in multiconfigurational SA-CASSCF calculations the active space of $\text{Im}-[\text{Co}^{\text{II}}(\text{corrin})]^+$ was comprised of 11 electrons distributed in 12 active orbitals, shown in Figure 4. Active orbitals were selected in SA-CASSCF in order to make comparison between the four-, and five-coordinate models, and to analyze the influence of the lower axial ligand.

The ground and four lowest excited states along with natural orbital compositions of $\text{Im}-[\text{Co}^{\text{II}}(\text{corrin})]^+$ obtained from the SA-CASSCF/ XMCQDPT2 calculations are collected in Table 2. It is important to mention that the XMCQDPT2 level of theory does not show mixing of CAS states, which is somehow different than the four-coordinate model. All five states observed at XMCQDPT2 retain the same order as that of their corresponding CASSCF states.

As shown in Table 2, the ground state wavefunction obtained with CASSCF/XMCQDPT2 has one dominant CSF with a weight contribution of 92%. This indicates that the unpaired electron of the $\text{Im}-[\text{Co}^{\text{II}}(\text{corrin})]^+$ model is mainly localized on the d_z^2 broadly in accord with the four-coordinate model. The most notable difference between the lower excited state manifolds of the four-, and five-coordinate models is a non-degeneracy of the D_0 and D_1 states, which is due to the presence of the imidazole ligand. The D_1 excited state of $\text{Im}-[\text{Co}^{\text{II}}(\text{corrin})]^+$ is composed of two dominant CSFs, $(d_{yz})^1(d_z^2)^2$, and $(d_{xz})^1(d_z^2)^2$, that contribute 55% and 31% to the XMCQDPT2 electronic state, respectively. This excited state is near degenerate in terms of both energy and electron configuration with the D_2 excited state. D_2 has two dominant CSFs with inverted weight percentages, $(d_{xz})^1(d_z^2)^2$, and $(d_{yz})^1(d_z^2)^2$ configurations, contributing 55% and 35% to the electronic state respectively. D_1 and D_2 are thus characterized as near degenerate $d_{yz/xz} \rightarrow d_z^2$ type transitions. The remaining low-lying excited states are also composed of

mixed d-d excitations, involving a d_z^2 acceptor orbital, with some minor d_z^2 contributions to each CSF. The D_3 excited state is characterized as mainly a $d_{x^2-y^2} \rightarrow d_z^2$ transition, composed of a 67% $(d_{x^2-y^2})^1(d_z^2)^2$ CSF, and a 16 % doubly excited $(d_{xz})^\uparrow (d_{yz})^\downarrow (d_z^2)^2(d_{xy-n})^\uparrow$ CSF. The 4th excited state has just one CSF, an 86% $(d_z^2)^0(d_{xy-n})^1$ configuration, characterized as $d_z^2 \rightarrow (d_{xy-n})$ transition.

The low-lying excited state manifold of the five-coordinate model determined by CASSCF/XMCQDPT2 was then used as a benchmark for comparison with TD-DFT using BP86/6-311G(d,p). Frontier orbitals of the unrestricted DFT wavefunction along with their corresponding orbital energies are collected in Figure S2, and corresponding TD-DFT excitation energies, along with their excited state characterizations are collected in Table S2. The frontier orbitals based on BP86/6-311G(d,p), contain a single occupied (SOMO) d_z^2 type orbital, labeled H(α ,113) consistent with SA-CASSCF/XMCQDPT2 calculations of Im-[Co^{II}(corrin)]⁺. As observed in the four-coordinated model, π electron density is present to some extent in all DFT frontier MOs, including in this case, the α d_z^2 MO, which has a small amount of π electron density from imidazole (Im).

To understand similarities between the lower excited state manifold of Im-[Co^{II}(corrin)]⁺ determined by both CASSCF and TD-DFT approaches, analysis of TD-DFT electronic transitions was carried out in terms of NTOs. NTOs of the lowest five states of the five-coordinate model are shown in Figure 5 (upper panel). The lowest excited states determined by both methods were composed of mixed d and π character, similar to the four-coordinated system, but were notably not exclusive to the β subspace. D_1 , D_3 , and D_4 excited electronic states determined by TD-DFT are d-d type transitions similar to lowest excited states determined by XMCQDPT. The D_2 state obtained in TD-DFT calculations arises from $d/\pi \rightarrow \pi^*$ excitation, and is not present in *ab initio* calculations. Transitions involving both occupied and unoccupied d_z^2 orbitals may be observed for the D_1 state calculated by TD-DFT, composed of both an α $d_z^2 + \pi$ donor orbital, and a β d_z^2 acceptor orbital, and characterized as a 69% of β $d_{yz} + \pi \rightarrow d_z^2 + \pi^*$, and 31% of α $d_z^2 + \pi_{im} \rightarrow \pi^*$ transition. D_3 state also include d_z^2 orbital contributions, and is characterized as a 17% of α $d_z^2 + \pi_{im}^*$, and 83% of β $d_{xz} + \pi \rightarrow d_z^2 + \pi^*$ transition. The D_1 and D_3 TD-DFT excited states are close in energy to each other, 1.40 and 1.59 eV respectively. This 0.2 eV difference in energy is relatively close to the difference in energy between D_1 and D_2 by SA-CASSCF/XMCQDPT2 (~0.1 eV). The D_4 TD-DFT excited state is very similar to D_3 but contains almost equal contributions from the α $d_z^2 + \pi_{im} \rightarrow \pi^*$, and β $d_{yz} + \pi \rightarrow d_z^2 + \pi^*$ transitions, as 52% and 48%, respectively. D_5 on the other hand, is a pure 92% β $d_{xz} + \pi_{im} \rightarrow \pi^*$ transition.

3.4. TD-DFT of the Full Structure of Cob(II)alamin

Comparison of the low-lying excited states between both four-, and five-coordinate models reveals comparable agreement between *ab-initio* CASSCF/XMCQDPT2 and TD-DFT methods. This benchmark study provides further confidence that TD-DFT calculations may be extended to full cobalamin structural models to accurately predict their electronically excited states. To evaluate the effects of truncation, TD-DFT was applied to cob(II)alamin to obtain the 10 lowest excited states at the BP86/6-311G(d,p) level. In addition, 160 states were obtained for cob(II)alamin at the BP86/SDD level to extend the range of states relevant to experiment at reduced computational cost. The experimental spectra of cob(II)alamin was taken from steady-state studies performed by the Sension group,³³ and is shown in Figure 6 with relevant TD-DFT states. Selected TD-DFT transitions of cob(II)alamin at the UBP86/SDD level, along with corresponding transitions for both minima and elongated Co-N states at the UBP86/6-311G(d,p) level are collected in Table 4. NTOs for these transitions are further collected in Figures S9, and S10. As may be seen, there is good correlation between experiment and TD-DFT excited states of cob(II)alamin, and the truncated models. Additionally, calculated TD-DFT transitions of cob(II)alamin are consistent with truncated models in energy, with some

subtle differences in the electronic character of their excited states. As may be noted in the NTOs of cob(II)alamin at the SDD level, the particle states are more delocalized than corresponding hole states, and is due to the treatment of the TD-DFT electron density using pseudopotentials, and TD-DFT NTO character for these states was determined by significant MO composition. Differences in oscillator strengths between the full and truncated minima in the range of around 2.7 eV to 3.0 eV of the calculated spectrum may be attributed to higher weight contributions of LF-type transitions observed in the truncated TD-DFT states. These transitions, are discussed with axial base dependence in Section 5.

The experimental transition around 2.7 eV, shown in Figure 6 is not significantly resolved in the TD-DFT spectra of the truncated minima, but comparable oscillator strengths for this transition is observed in both the full model, and the LF state of the truncated model. We then, as a next step investigated this electronic transition to explore the nature of these excited states. This is shown in Table 4, and further in Figures S8 and S10, where the D_{19} state of the full structure at the UBP86/SDD level, and D_{17} state of the truncated model complex at the BP86/6-311G(d,p) level both show the transition around 2.7 eV, with appreciable oscillator strengths. This transition, which is associated with $d_z^2 + \pi \rightarrow \pi^*$ character, appears in the D_{23} state of the truncated model with 17% contribution, which has notable oscillator strength around 3.0 eV (Figure S9). This $d_z^2 + \pi \rightarrow \pi^*$ transition also occurs as a 25% weight contribution to D_{19} state for the full structure of cob(II)alamin, and essentially composes 100% of the LF excited state (D_{17}) by partitioning between α and β subspaces, as a β $d_z^2 + \pi \rightarrow \pi^*$ (58%), α $d_z^2 + \pi \rightarrow \pi^*$ (42%) transition.

NTOs of the lowest five TD-DFT excited states of cob(II)alamin at the UBP86/6-311G(d,p) level are shown in Figure 7, and further through D_{10} in Figure S4. The most apparent difference at the TD-DFT level between the five lowest excited states of cob(II)alamin, and the truncated model (Figure 5, upper panel), is the reverse the order energy for D_2 and D_3 electronic states. In the case of the full structure of cob(II)alamin, there is a decrease in α d_z^2 character of the lower two excited states. The D_1 state of cob(II)alamin occurs with less α d_z^2 character than Im-[Co^{II}(corrin)]⁺ model complex (6% vs. 31%, respectively), and the D_2 state occurs with a 100% β d_z^2 acceptor MO, and no α contribution. The remaining low-lying excited states of cob(II)alamin and the model complex are readily verified as consistent with each other in character, as a 63% of $d_{yz} + \pi \rightarrow \pi^*$, 37% of $d_{yz} + \pi_{im} \rightarrow \pi^*$ transition for the D_3 state, a 91% of $d_z^2 + \pi_{im} \rightarrow \pi^*$, 8% of $d_{yz} + \pi \rightarrow \pi^*$ transition for the D_4 state, and an 85% of $d_{xz} + \pi \rightarrow \pi^*$, 14% of $d_{xz} + \pi \rightarrow \pi^*$, transition for the D_5 state. It may also be noted that the optimized Co- N_{im} bond distance for cob(II)alamin is slightly longer than that of the truncated model, 2.23 Å vs 2.13 Å, respectively. This elongation of Co-N bond length could be attributed to the additional electron density of the full system where cobalt, corrin, and DBI are included, and may be attributed to larger a repulsive interaction of the DBI ligand with the equatorial coordination sphere in the full structure, when compared to the interaction of imidazole in the model complex. The effects of the 6-311G(d,p) and the SDD pseudopotential basis sets on the electronic structures corresponding to the full model may be seen in Figure S5. Frontier orbitals, and the lowest five cob(II)alamin NTOs calculated with SDD basis sets are collected in Figures S6, and S7. It may be seen that the LUMO and $L + 1$ β MOs at the UBP86/SDD level are consistent with the character of lower excited states of the truncated model calculated with the 6-311G(d,p) basis set. It is important to mention that the D_1 state at the TD-DFT level is consistently a transition to the d_z^2 orbital, regardless of basis set, structural model, or whether the d_z^2 orbital is LUMO or $L + 1$. As discussed in section 3.5, an increase in Co- N_{im} bond-length can be summarized as corresponding to lowering of energy of the d_z^2 orbital in both subspaces α and β , which effectively leads to a decrease in α $d_z^2 \rightarrow \pi^*$ character, and an increase in β $d_{yz} + \pi \rightarrow d_z^2$ character of the D_1 excited states for the five coordinated complex. At longer Co- N_{im} distances two LF excited states are

close in energy with small excitation energy, and correspond to the two low-lying LF states for four-coordinate complex (D_1 and D_2 states in Table 3 and Table S1).

Although subtle differences in electronic character of frontier orbitals may be noted between the full and truncated models, the energies of these transitions relative to their respective ground states are comparable, with oscillator strengths also comparable to experimental spectra, and as such these calculations should be considered reliable for the prediction of excited state properties.

3.5. Electronic Structure of Low-Lying Ligand Field States: Influence of Axial Base

Consistency between TD-DFT and *ab-initio* CASSCF/XMCQDPT2 methods for both four- and five-coordinated models, as well as consistency between the TD-DFT states of the full cob(II)alamin structure, and the truncated models, further validates the accuracy of calculated TD-DFT excited states in the ligand-field range. To further understand the electronic structure, and the nature of low-lying excited cob(II)alamin states as a function of axial base, DFT/UBP86 was applied to the five-coordinated model as described, and obtain frontier MOs as a function of axial base (Figure 8). The most notable feature of $[\text{Co}^{\text{II}}(\text{corrin})]^+$ with respect to elongation of the Co- N_{im} distance (Figure 8), is the lowering in energy of both α and β $d_z^2 + \pi$ orbitals in the LF space. This is in agreement with a system approaching the four-coordinate structural model, where the β $d_z^2 + \pi$ is the LUMO, and much closer in energy to the occupied orbitals. In Co- N_{im} distances where the lowest electronic state has dominant LF character, the energy of the $d_z^2 + \pi_{\text{im}}$ MO is also lower in the alpha subspace, and for a distances around 2.80 Å, corresponds to α H-4, with all other frontier orbitals remaining essentially unchanged with respect to the Co-N coordinate. The band gap in the LF state of the five-coordinate model was also lower than at the minimum, 1.10 eV vs. 1.57 eV respectively, between β MOs $d_{yz} + \pi$ and $d_z^2 + \pi_{\text{im}}^*$, rather than α MOs $d_z^2 + \pi_{\text{im}}$ and π^* at the minima. Although the five-coordinate LF model, and the four coordinate model have HOMOs and LUMOs consistent with each other, a lower band gap of 0.45 eV is observed for the four-coordinate model. The lowering of D_1 excitation energy with respect to Co- N_{im} distance, is shown in Figure 9, and is associated with an increase in β $d_{yz} + \pi \rightarrow d_z^2$ excited state character. As shown in Figure 9, decreasing the Co- N_{im} bond length to 1.85 Å lowers the D_1 energy, with an increase in α d_z^2 ground state that contributes to a 100% α $d_z^2 + \pi_{\text{im}} \rightarrow \pi^*$ transition. NTOs for these lowest 5 TD-DFT states corresponding to a Co- N_{im} bond length of 1.85 Å are collected in Table S5, and shown in Figure S3.

NTOs of the lower excited state manifold of the LF state are shown in Figure 5 (lower panel), and consist mainly of transitions to d_z^2 orbitals of the β subspace, with minor contributions from the α π^* acceptor. The D_1 and D_2 NTOs are exclusively comprised of the β subspace consistent with four-coordinated cob(II)alamin, and have very low excitation energies, 0.72 and 0.91 eV, respectively. The remaining three low-lying excited states can be described as having minor α $\pi \rightarrow \pi^*$ character, with higher weight contributions from β transitions, to a d_z^2 acceptor. This is also observed in D_4 and D_5 of the lower LF excited states shown in Figure 5 (lower panel). D_4 is essentially composed of the same α and β MOs as D_3 , but it is higher in energy, 1.55 versus 1.66 eV respectively, with a higher weight from the α $\pi \rightarrow \pi^*$ transition. The- D_5 electronic state, which has three π and π^* components, can be characterized as mainly a $\pi \rightarrow d_z^2$ (92%) transition.

TD-DFT states with simultaneous ground and excited state contributions from the d_z^2 MO may also be noted throughout the lower excited state manifolds of the full structure and five-coordinate minima in Table 4, around 2.71 eV (D_{19}), and 3.00 eV (D_{23}). This difference in energy is mainly attributed to structure size as may be expected, and may be validated at the BP86/6-311G (d,p) level of theory between the two models (Table S2, and Figure S4). The α $d_z^2 + \pi \rightarrow \pi^*$ component, may also be noted in the LF excited state (D_{17}) around 2.73 eV, along with a symmetric 58% β $d_z^2 + \pi \rightarrow \pi^*$ component, indicating that some LF character is inherent in the ground state at this energy.

Summary and Conclusions

The electronically excited states of Co(II) do not play a role in thermal processes, as they are mediated by the ground state. However, the electronically excited states of Co(II) are very important for cobalamin photochemistry, as may be exemplified in recent studies of MeCbl where photocleavage involves excited states cob(II)alamin. The most important outcome of the present study was the simulated spectrum (Figure 6), which reproduced experiment very well. Although a number of low-lying transitions below 2.0 eV are predicted at *ab-initio* and TD-DFT levels that cannot be observed in the Abs spectrum, several features in MCD data previously reported can be reasonably correlated with our predictions.¹² These transitions which are not observed in the absorption spectrum, may be correlated with MCD spectrum with further experimental efforts.

A new predicted feature of this study is the nature of the D_1 state, which shows a mixed d_z^2 donor and acceptor character as a function of axial base distance, which may be directly attributed to the lowering in energy of the d_z^2 unoccupied orbitals. Detachment of axial base from the Co(II) corrin complex should thus lead to near degeneration of low-lying LF $d \rightarrow d_z^2$ electronic states with the ground state. This is an intriguing observation implying that long Co- N_{axial} bond distances correspond to a ligand-field state. Further confirmations by experiment regarding this state would be insightful.

Acknowledgments

This work was supported by the National Science Centre, Poland, under grant no. UMO-2013/09/B/ST4/03014. Calculations performed using TURBOMOLE were carried out in the Wroclaw Centre for Networking and Supercomputing, WCSS, Wroclaw, Poland, <http://www.wcss.wroc.pl>, under calculational grant no. 18. We are also very thankful to Professor R. J. Sension for providing experimental spectrum in digital form. Visiting professorship of Pawel M. Kozlowski at the Medical University of Gdansk was partially supported by the KNOW program.

Reference

1. D. Dolphin, *B12*, John Wiley & Sons, New York 1982.
2. B. Krautler, D. Arigoni and B. T. E. Golding, *Vitamin B₁₂ and B₁₂ Proteins*, Wiley-VCH, New York, 1998.
3. R. Banerjee, *Chemistry and Biochemistry of B12*, John Wiley & Sons, New York, 1999.
4. H. P. C. Hogenkamp, H. A. Barker and H. S. Mason, *Archives of Biochemistry and Biophysics*, 1963, **100**, 353-359.
5. G. N. Schrauzer and L.-P. Lee, *Journal of the American Chemical Society*, 1968, **90**, 6541-6543.
6. J. H. Bayston, F. D. Looney, J. R. Pilbrow and M. E. Winfield, *Biochemistry*, 1970, **9**, 2164-2172.
7. E. Joerin, A. Schweiger and H. H. Guenthard, *Journal of the American Chemical Society*, 1983, **105**, 4277-4286.
8. S.-C. Ke, M. Torrent, D. G. Museav, K. Morokuma and K. Warncke, *Biochemistry*, 1999, **38**, 12681-12689.
9. J. S. Trommel, K. Warncke and L. G. Marzilli, *Journal of the American Chemical Society*, 2001, **123**, 3358-3366.
10. J. Harmer, S. Van Doorslaer, I. Gromov and A. Schweiger, *Chemical Physics Letters*, 2002, **358**, 8-16.
11. S. Van Doorslaer, G. Jeschke, B. Epel, D. Goldfarb, R.-A. Eichel, B. Kräutler and A. Schweiger, *Journal of the American Chemical Society*, 2003, **125**, 5915-5927.
12. T. A. Stich, N. R. Buan and T. C. Brunold, *Journal of the American Chemical Society*, 2004, **126**, 9735-9749.
13. M. D. Liptak, A. S. Fleischhacker, R. G. Matthews, J. Telser and T. C. Brunold, *The Journal of Physical Chemistry B*, 2009, **113**, 5245-5254.
14. M. D. Liptak, S. Datta, R. G. Matthews and T. C. Brunold, *Journal of the American Chemical Society*, 2008, **130**, 16374-16381.
15. B. Krautler, W. Keller and C. Kratky, *Journal of the American Chemical Society*, 1989, **111**, 8936-8938.
16. R. Padmakumar and R. Banerjee, *Biochemistry*, 1997, **36**, 3713-3718.
17. E. N. G. Marsh and D. P. Ballou, *Biochemistry*, 1998, **37**, 11864-11872.
18. S. S. Licht, S. Booker and J. A. Stubbe, *Biochemistry*, 1999, **38**, 1221-1233.
19. V. Bandarian and G. H. Reed, *Biochemistry*, 2000, **39**, 12069-12075.
20. M. Wang and K. Warncke, *Journal of the American Chemical Society*, 2008, **130**, 4846-4858.
21. G. Gerfen, in *Chemistry and Biochemistry of B12*, ed. R. Banerjee, John Wiley & Sons, New York, 1999, ch. 165-195.
22. R. G. Matthews, *Accounts of Chemical Research*, 2001, **34**, 681-689.
23. R. G. Matthews, M. Koutmos and S. Datta, *Current Opinion in Structural Biology*, 2008, **18**, 658-666.
24. M. Koutmos, S. Datta, K. A. Patridge, J. L. Smith and R. G. Matthews, *Proceedings of the National Academy of Sciences*, 2009, **106**, 18527-18532.
25. M. Kumar and P. M. Kozlowski, *Angewandte Chemie International Edition*, 2011, **50**, 8702-8705.
26. M. Kumar, N. Kumar, H. Hirao and P. M. Kozlowski, *Inorganic Chemistry*, 2012, **51**, 5533-5538.
27. J. C. Escalante-Semerena, S. J. Suh and J. R. Roth, *Journal of Bacteriology*, 1990, **172**, 273-280.
28. T. A. Stich, N. R. Buan, J. C. Escalante-Semerena and T. C. Brunold, *Journal of the American Chemical Society*, 2005, **127**, 8710-8719.
29. M. St Maurice, P. E. Mera, M. P. Taranto, F. Sesma, J. C. Escalante-Semerena and I. Rayment, *Journal of Biological Chemistry*, 2007, **282**, 2596-2605.

30. N. R. Buan, S. J. Suh and J. C. Escalante-Semerena, *Journal of Bacteriology*, 2004, **186**, 5708-5714.
31. E. Chen and M. R. Chance, *Biochemistry*, 1993, **32**, 1480-1487.
32. L. A. Walker, J. J. Shiang, N. A. Anderson, S. H. Pullen and R. J. Sension, *Journal of the American Chemical Society*, 1998, **120**, 7286-7292.
33. L. A. Walker, J. T. Jarrett, N. A. Anderson, S. H. Pullen, R. G. Matthews and R. J. Sension, *Journal of the American Chemical Society*, 1998, **120**, 3597-3603.
34. J. J. Shiang, L. A. Walker, N. A. Anderson, A. G. Cole and R. J. Sension, *The Journal of Physical Chemistry B*, 1999, **103**, 10532-10539.
35. L. M. Yoder, A. G. Cole, L. A. Walker and R. J. Sension, *The Journal of Physical Chemistry B*, 2001, **105**, 12180-12188.
36. A. G. Cole, L. M. Yoder, J. J. Shiang, N. A. Anderson, L. A. Walker, M. M. Banaszak Holl and R. J. Sension, *Journal of the American Chemical Society*, 2002, **124**, 434-441.
37. R. J. Sension, D. A. Harris and A. G. Cole, *The Journal of Physical Chemistry B*, 2005, **109**, 21954-21962.
38. R. J. Sension, D. A. Harris, A. Stickrath, A. G. Cole, C. C. Fox and E. N. G. Marsh, *The Journal of Physical Chemistry B*, 2005, **109**, 18146-18152.
39. J. J. Shiang, A. G. Cole, R. J. Sension, K. Hang, Y. Weng, J. S. Trommel, L. G. Marzilli and T. Lian, *Journal of the American Chemical Society*, 2006, **128**, 801-808.
40. D. A. Harris, A. B. Stickrath, E. C. Carroll and R. J. Sension, *Journal of the American Chemical Society*, 2007, **129**, 7578-7585.
41. A. B. Stickrath, E. C. Carroll, X. Dai, D. A. Harris, A. Rury, B. Smith, K.-C. Tang, J. Wert and R. J. Sension, *The Journal of Physical Chemistry A*, 2009, **113**, 8513-8522.
42. J. Peng, K.-C. Tang, K. McLoughlin, Y. Yang, D. Forgach and R. J. Sension, *The Journal of Physical Chemistry B*, 2010, **114**, 12398-12405.
43. A. S. Rury, T. E. Wiley and R. J. Sension, *Accounts of Chemical Research*, 2015, **48**, 860-867.
44. L. Randaccio, M. Furlan, S. Geremia, M. Šlouf, I. Srnova and D. Toffoli, *Inorganic Chemistry*, 2000, **39**, 3403-3413.
45. L. Randaccio, S. Geremia, G. Nardin and J. Wuerges, *Coordination Chemistry Reviews*, 2006, **250**, 1332-1350.
46. T. B. Demissie, M. Repisky, H. Liu, K. Ruud and P. M. Kozlowski, *Journal of Chemical Theory and Computation*, 2014, **10**, 2125-2136.
47. A. D. Becke, *Physical Review A*, 1988, **38**, 3098-3100.
48. J. P. Perdew, *Physical Review B*, 1986, **33**, 8822-8824.
49. E. Van Lenthe and E. J. Baerends, *Journal of Computational Chemistry*, 2003, **24**, 1142-1156.
50. E. van Lenthe, A. Ehlers and E. J. Baerends, *Journal of Chemical Physics*, 1999, **110**, 8943-8953.
51. *Amsterdam Density Functional*, 2012, Vrije Universiteit, available from <http://www.scm.com>.
52. *TURBOMOLE*, 2014, a development of University of Karlsruhe and Forschungszentrum Karlsruhe GmbH, 1989–2007, TURBOMOLE GmbH, since 2007; available from <http://www.turbomole.com>.
53. M. J. G. Frisch, W. Trucks, H. B. Schlegel, G. E. Scuseria, M. A. Robb, J. R. Cheeseman, G. Scalmani, V. Barone, B. G. Mennucci, A. Petersson, H. Nakatsuji, M. Caricato, X. Li, H. P. Hratchian, A. F. Izmaylov, J. Bloino, G. Zheng, J. L. Sonnenberg, M. E. M. Hada, K. Toyota, R. Fukuda, J. Hasegawa, M. Ishida, T. Nakajima, Y. Honda, O. Kitao, H. Nakai, T. Vreven, J. A. Montgomery, J. E. Peralta, F. Ogliaro, M. Bearpark, J. J. Heyd, E. Brothers, K. N. Kudin, V. N. Staroverov, R. Kobayashi, J. Normand, K. Raghavachari, A. Rendell, J. C. Burant, S. S. Iyengar, J. Tomasi, M. Cossi, N. Rega, J. M. Millam, M. Klene, J. E. Knox, J. B. Cross, V. Bakken, C. Adamo, J. Jaramillo, R. Gomperts, R. E. Stratmann, O. Yazyev, A. J. Austin, R. Cammi, C. Pomelli, J. W. Ochterski, R. L. Martin, K. Morokuma, V. G. Zakrzewski, G. A. Voth, P. Salvador, J. J. Dannenberg, S. Dapprich, A. D. Daniels, O. Farkas, J. B. Foresman, J. V. Ortiz, J. Cioslowski and D. J. Fox (Gaussian 09).

54. R. L. Martin, *Journal of Chemical Physics*, 2003, **118**, 4775-4777.
55. A. A. Granovsky, *Firefly Version 8.0.0*, <http://classic.chem.msu.su/gran/firefly/index.html>
56. A. A. Granovsky, *Journal of Chemical Physics*, 2011, **134**.
57. H. Nakano, *Journal of Chemical Physics*, 1993, **99**, 7983-7992.
58. K. Kornobis, N. Kumar, B. M. Wong, P. Lodowski, M. Jaworska, T. Andruniow, K. Ruud and P. M. Kozlowski, *Journal of Physical Chemistry A*, 2011, **115**, 1280-1292.
59. K. Kornobis, N. Kumar, P. Lodowski, M. Jaworska, P. Piecuch, J. J. Lutz, B. M. Wong and P. M. Kozlowski, *Journal of Computational Chemistry*, 2013, **34**, 987-1004.
60. P. M. Kozlowski, T. Kamachi, M. Kumar, T. Nakayama and K. Yoshizawa, *Journal of Physical Chemistry B*, 2010, **114**, 5928-5939.
61. N. Kumar, M. Jaworska, P. Lodowski, M. Kumar and P. M. Kozlowski, *Journal of Physical Chemistry B*, 2011, **115**, 6722-6731.
62. N. Kumar, M. Alfonso-Prieto, C. Rovira, P. Lodowski, M. Jaworska and P. M. Kozlowski, *Journal of Chemical Theory and Computation*, 2011, **7**, 1541-1551.
63. N. Kumar, J. Kuta, W. Galezowski and P. M. Kozlowski, *Inorganic Chemistry*, 2013, **52**, 1762-1771.
64. N. Kumar and P. M. Kozlowski, *Journal of Physical Chemistry B*, 2013, **117**, 16044-16057.

Table 1. The lowest five states of $[\text{Co}^{\text{II}}(\text{corrin})]^+$ obtained from CASSCF/XMCQDPT2 calculations, where CSF denotes the configuration state function.

State	eV	f	Weight (%) of CAS state in XMCQDPT2	CAS state	Weight of CSF [%]	Electronic configuration of CAS state	Character
D ₀	0.00		75	1	94	$(d_z^2)^1$	$d_{yz} \rightarrow d_z^2$
			25	2	85	$(d_{yz})^1(d_z^2)^2$	
D ₁	0.01	0.00000	25	1	94	$(d_z^2)^1$	$d_{yz} \rightarrow d_z^2$
			75	2	85	$(d_{yz})^1(d_z^2)^2$	
D ₂	1.35	0.00000	99	3	68	$(d_{x^2-y^2})^1(d_z^2)^2$	$d_{x^2-y^2} \rightarrow d_z^2$
					15	$(d_{xz})^\uparrow(d_{yz})^\downarrow(d_z^2)^2(d_{xy-n})^\uparrow$	$d_{xz}/d_{yz} \rightarrow d_z^2/d_{xy-n}$
D ₃	2.05	0.00001	98	4	35	$(d_{x^2-y^2})^\uparrow(d_{xz})^\downarrow(d_z^2)^2(d_{xy-n})^\uparrow$	$d_{x^2-y^2}/d_{xz} \rightarrow d_z^2/d_{xy-n}$
					26	$(d_{x^2-y^2})^\uparrow(d_{xz})^\uparrow(d_z^2)^2(d_{xy-n})^\downarrow$	$d_{x^2-y^2}/d_{xz} \rightarrow d_z^2/d_{xy-n}$
					18	$(d_{xz})^\uparrow(d_z^2)^\downarrow(d_{xy-n})^\uparrow$	$d_{xz} \rightarrow d_{xy-n}$
					11	$(d_{xz})^\uparrow(d_z^2)^\uparrow(d_{xy-n})^\downarrow$	$d_{xz} \rightarrow d_{xy-n}$
D ₄	2.18	0.00001	99	5	62	$(d_{xz})^\uparrow(d_{yz})^\downarrow(d_z^2)^2(d_{xy-n})^\uparrow$	$d_{xz}/d_{yz} \rightarrow d_z^2/d_{xy-n}$
					23	$(d_{xz})^\uparrow(d_{yz})^\uparrow(d_z^2)^2(d_{xy-n})^\downarrow$	$d_{xz}/d_{yz} \rightarrow d_z^2/d_{xy-n}$

Table 2. The lowest five states of $[\text{Im-Co}^{\text{II}}(\text{corrin})]^+$ obtained from CASSCF/ XMCQDPT2 calculations, where CSF denotes the configuration state function.

State	eV	f	Weight (%) of CAS state in XMCQDPT2	CAS state	Weight of CSF [%]	Electronic configuration of CAS state	Character
D ₀	0.00		100	1	92	$(d_z^2)^1$	
D ₁	0.90	0.00009	96	2	55 31	$(d_{yz})^1(d_z^2)^2$ $(d_{xz})^1(d_z^2)^2$	$d_{yz} \rightarrow d_z^2$ $d_{xz} \rightarrow d_z^2$
D ₂	1.03	0.00012	96	3	55 31	$(d_{xz})^1(d_z^2)^2$ $(d_{yz})^1(d_z^2)^2$	$d_{xz} \rightarrow d_z^2$ $d_{yz} \rightarrow d_z^2$
D ₃	2.09	0.00001	95	4	67 16	$(d_{x^2-y^2})^1(d_z^2)^2$ $(d_{xz})^1(d_{yz})^1(d_{zz})^2(d_{xy-n})^1$	$d_{x^2-y^2} \rightarrow d_z^2$ $d_{xz}/d_{yz} \rightarrow d_z^2/d_{xy-n}$
D ₄	2.87	0.00004	100	5	86	$(d_{zz})^0(d_{xy-n})^1$	$d_z^2 \rightarrow d_{xy-n}$

Table 3. The 10 lowest excited states of $[\text{Im}^- - \text{Co}^{\text{II}}(\text{corrin})]^+_{(2.80 \text{ \AA})}$ obtained from TD-DFT BP86/6-311G(d,p) calculations.

State	eV	$\lambda(\text{nm})$	f	NTO Coeff.	TD-DFT Character		
D ₀	0.00			100			$(d_{z^2})^1$
D ₁	0.72	1731.4	0.0000	100	112(β) \rightarrow 113(β)	H(β) \rightarrow L(β)	$d_{yz} + \pi \rightarrow d_z^2 + \pi_{\text{Im}}^*$
D ₂	0.91	1360.1	0.0000	100	111(β) \rightarrow 113(β)	H-1(β) \rightarrow L+1(β)	$d_{xz} + \pi \rightarrow \pi^*$
D ₃	1.55	800.1	0.0017	11	113(α) \rightarrow 114(α)	H(α) \rightarrow L(α)	$\pi \rightarrow \pi^*$
				52	110(β) \rightarrow 113(β)	H-2(β) \rightarrow L(β)	$d_{x^2-y^2} \rightarrow d_z^2 + \pi_{\text{Im}}^*$
				37	112(β) \rightarrow 114(β)	H(β) \rightarrow L+1(β)	$d_{yz} + \pi \rightarrow \pi^*$
D ₄	1.66	745.0	0.0001	25	113(α) \rightarrow 114(α)	H(α) \rightarrow L(α)	$\pi \rightarrow \pi^*$
				50	110(β) \rightarrow 113(β)	H-2(β) \rightarrow L(β)	$d_{x^2-y^2} \rightarrow d_z^2 + \pi_{\text{Im}}^*$
				25	112(β) \rightarrow 114(β)	H(β) \rightarrow L+1(β)	$d_{yz} + \pi \rightarrow \pi^*$
D ₅	1.84	672.4	0.0015	8	113(α) \rightarrow 114(α)	H(α) \rightarrow L(α)	$\pi \rightarrow \pi^*$
				92	109(β) \rightarrow 113(β)	H(β) \rightarrow L(β)	$\pi \rightarrow d_z^2 + \pi_{\text{Im}}^*$
D ₆	1.97	629.3	0.0030	6	111(α) \rightarrow 114(α)	H-2(α) \rightarrow L(α)	$d_{xz} + \pi \rightarrow \pi^*$
				94	111(β) \rightarrow 114(β)	H(β) \rightarrow L+2(β)	$d_{xz} + \pi \rightarrow \pi^*$
D ₇	2.24	554.6	0.0000	59	113(α) \rightarrow 115(α)	H(α) \rightarrow L+1(α)	$\pi \rightarrow d_{xy-n}$
				41	112(β) \rightarrow 114(β)	H(β) \rightarrow L+2(β)	$d_{yz} + \pi \rightarrow d_{xy-n}$
D ₈	2.26	549.0	0.0001	14	110(α) \rightarrow 114(α)	H-3(α) \rightarrow L(α)	$d_{x^2-y^2} \rightarrow \pi^*$
				86	110(β) \rightarrow 114(β)	H-2(β) \rightarrow L+2(β)	$d_{x^2-y^2} \rightarrow \pi^*$
D ₉	2.26	547.6	0.0004	55	112(α) \rightarrow 114(α)	H-1(α) \rightarrow L(α)	$d_z^2 + \pi \rightarrow \pi^*$
				45	110(β) \rightarrow 114(β)	H-2(β) \rightarrow L+1(β)	$d_{x^2-y^2} \rightarrow \pi^*$
D ₁₀	2.29	540.4	0.0000	100	108(β) \rightarrow 113(β)	H-4(β) \rightarrow L(β)	$\pi_{\text{Im}} \rightarrow d_z^2 + \pi_{\text{Im}}^*$

Table 4. Select TDDFT excited states of the full cob(II)alamin structure using BP86/SDD, and truncated models $[\text{Im-Co}^{\text{II}}(\text{corrin})]^+$ (min, 2.13 Å), and $[\text{Im} - - \text{Co}^{\text{II}}(\text{corrin})]^+$ (LF, 2.80 Å) using BP86/6-311G(d,p).

State	eV	λ (nm)	f	NTO Coeff.	major TDDFT MOs	Character
cob(II)alamin (min, 2.23 Å)						
D ₁₉	2.71	457.2	0.0276	46	251(α) \rightarrow 255(α)	$d_{x^2-y^2} + \pi \rightarrow \pi^*$
				29	250(β) \rightarrow 255(β)	$d_{x^2-y^2} + \pi \rightarrow d_{z^2} + \pi_{\text{Im}}^*$
				25	254(α) \rightarrow 257(α)	$d_z^2 + \pi \rightarrow \pi^*$
D ₂₉	2.93	422.9	0.0377	63	247(α) \rightarrow 255(α)	$\pi_{\text{Im}} + p \rightarrow \pi^*$
				19	246(α) \rightarrow 255(α)	$\pi + d_z^2 \rightarrow \pi^*$
				19	247(β) \rightarrow 254(β)	$\pi_{\text{Im}} \rightarrow \pi^*$
D ₆₁	3.39	366.2	0.0263	78	252(β) \rightarrow 258(β)	$d_{xz} + \pi \rightarrow \pi^*$
				22	252(α) \rightarrow 258(α)	$d_{xz} + \pi_{\text{Im}} \rightarrow \pi^*$
D ₁₄₄	3.95	313.7	0.0923	60	250(β) \rightarrow 259(β)	$d_{x^2-y^2} + \pi \rightarrow d_{xy-n}$
				40	242(α) \rightarrow 257(α)	$\pi_p \rightarrow \pi^*$
$[\text{Im-Co}^{\text{II}}(\text{corrin})]^+$ (min, 2.13 Å)						
D ₂₃	3.00	413.8	0.0610	32	109(α) \rightarrow 114(α)	$\pi + d_z^2 \rightarrow \pi^*$
				17	113(α) \rightarrow 117(α)	$d_z^2 + \pi \rightarrow \pi^*$
				30	110(β) \rightarrow 115(β)	$d_{x^2-y^2} \rightarrow d_{xy-n}$
				21		$\pi \rightarrow d_{z^2} + \pi^*$
D ₃₃	3.38	366.7	0.0500	75	111(β) \rightarrow 117(β)	$d_{xz} + \pi \rightarrow \pi^*$
				25	110(α) \rightarrow 115(α)	$d_{x^2-y^2} \rightarrow d_{xy-n}$
D ₄₅	3.80	326.1	0.0689	89	111(α) \rightarrow 117(α)	$d_{xz} + \pi + \pi_{\text{Im}} \rightarrow \pi^*$
					108(α) \rightarrow 115(α)	
				11	112(β) \rightarrow 114(β)	$d_{xz} + \pi \rightarrow \pi^*$
D ₅₆	4.09	303.0	0.2433	40	109(α) \rightarrow 116(α)	$\pi + d_z^2 \rightarrow \pi^*$
				33	109(β) \rightarrow 115(β)	$\pi + d_z^2 \rightarrow \pi^*$
				15	106(β) \rightarrow 114(β)	$\pi \rightarrow d_{yz} + \pi^*$
				12		$\pi + d_{yz} \rightarrow \pi^*$
$[\text{Im} - - \text{Co}^{\text{II}}(\text{corrin})]^+$ (LF, 2.80 Å)						
D ₁₇	2.73	455.0	0.0455	58	112(α) \rightarrow 114(α)	$d_z^2 + \pi \rightarrow \pi^*$
					109(α) \rightarrow 114(α)	
				42	109(β) \rightarrow 114(β)	$d_z^2 + \pi \rightarrow \pi^*$
D ₂₆	3.09	401.2	0.0953	66	109(α) \rightarrow 114(α)	$\pi + d_z^2 \rightarrow \pi^*$
				34	109(β) \rightarrow 114(β)	$d_{x^2-y^2} \rightarrow \pi^*$
D ₃₃	3.44	360.0	0.0520	74	105(β) \rightarrow 113(β)	$\pi_{\text{Im}} + p \rightarrow d_z^2 + \pi_{\text{Im}}^*$
				26	109(α) \rightarrow 115(α)	$\pi + d_z^2 \rightarrow d_{xy-n}$
D ₅₄	4.06	305.1	0.2472	40	109(α) \rightarrow 116(α)	$\pi + d_z^2 \rightarrow \pi^*$
				33	109(β) \rightarrow 115(β)	$\pi + d_z^2 \rightarrow \pi^*$
				15	107(α) \rightarrow 114(α)	$\pi + d_{yz} \rightarrow \pi^*$
				12	107(β) \rightarrow 114(β)	$\pi + d_{yz} \rightarrow \pi^*$

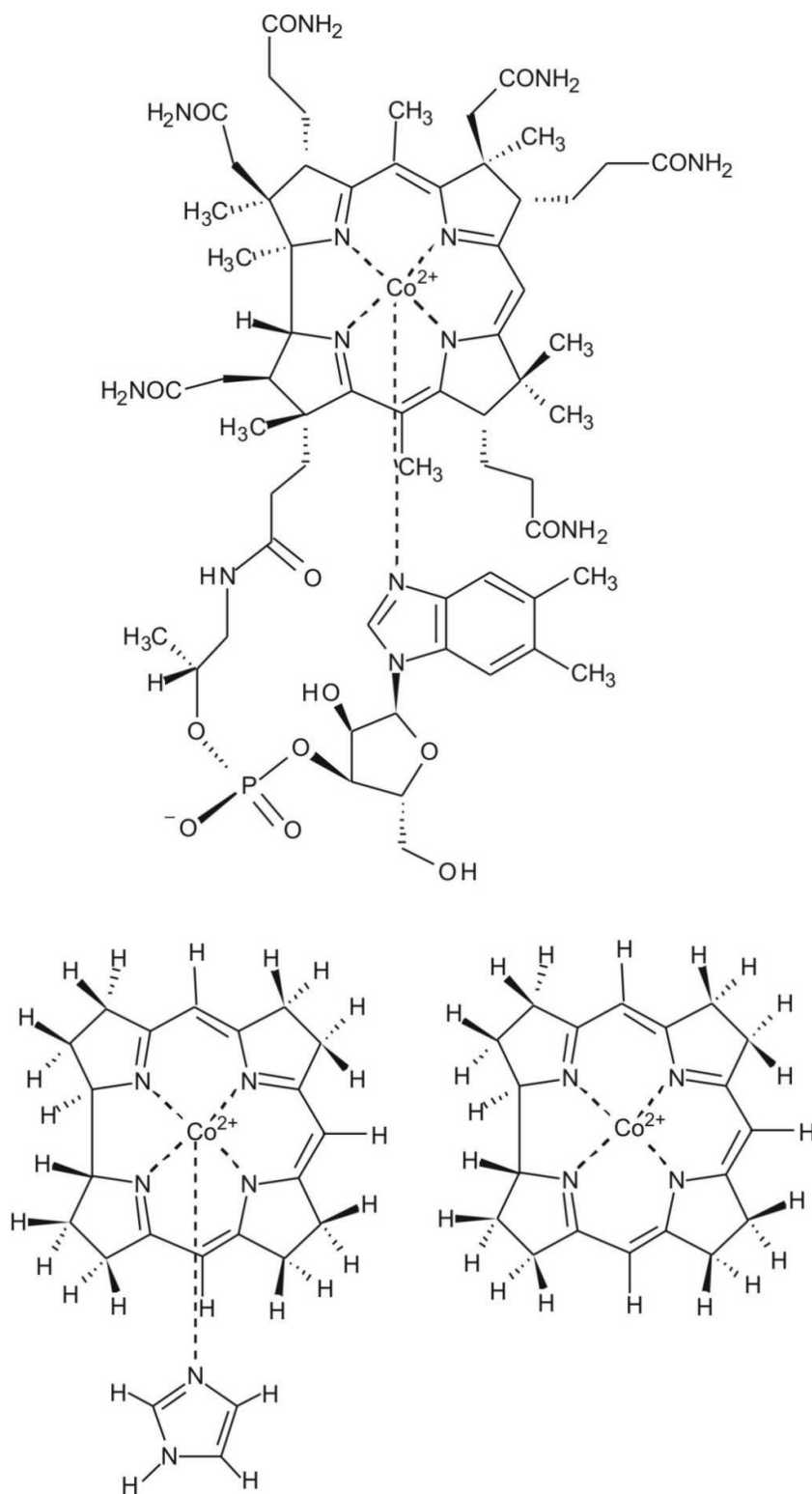


Figure 1. Molecular structure of the co(II)balamin and corresponding structural models.

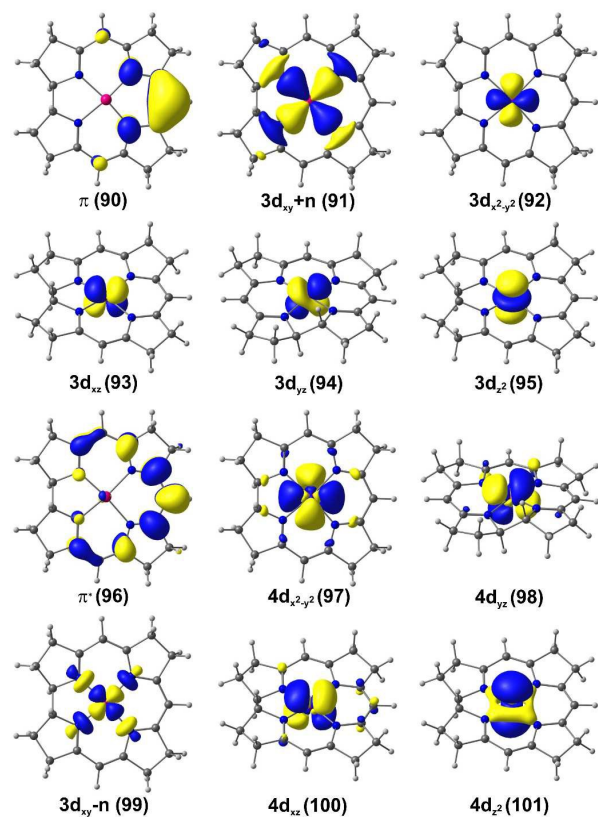
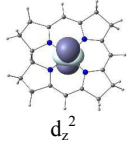
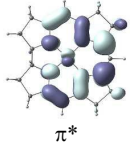
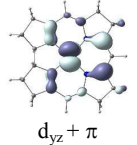
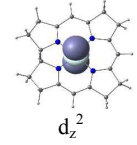
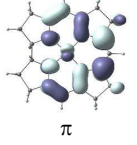
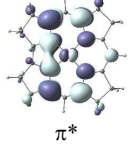
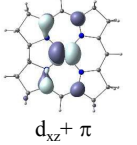
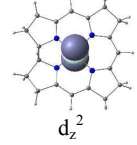
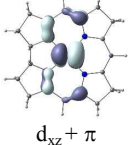
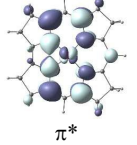
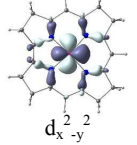
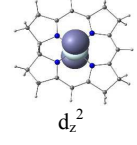
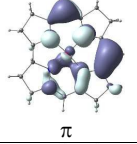
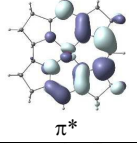
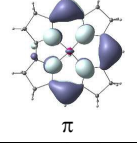
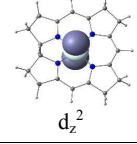
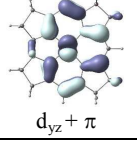
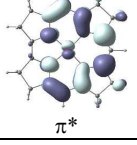
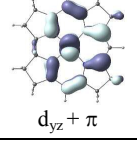
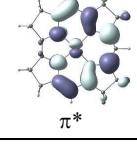


Figure 2. Active space corresponding to $[\text{Co}^{\text{II}}(\text{corrin})]^+$ used in the CASSCF(11,12) and subsequent XMCQDPT2 calculations.

Figure 3. Natural Transition Orbitals (NTOs) for $[\text{Co}^{\text{II}}(\text{corrin})]^+$ based on TD-DFT calculations at the uBP86/6-311G(d,p) level.

NTO	eV	NTO Coeff	f	α hole	α particle	β hole	β particle
D ₁	0.45	0 (α) 100 (β)	0.0000	 d_z^2	 π^*	 $d_{yz} + \pi$	 d_z^2
D ₂	0.68	0 (α) 100 (β)	0.0000	 π	 π^*	 $d_{xz} + \pi$	 d_z^2
D ₃	1.38	0 (α) 99 (β)	0.0007	 $d_{xz} + \pi$	 π^*	 $d_x^2 - d_y^2$	 d_z^2
D ₄	1.52	0 (α) 99 (β)	0.0003	 π	 π^*	 π	 d_z^2
D ₅	2.13	39 (α) 61 (β)	0.0005	 $d_{yz} + \pi$	 π^*	 $d_{yz} + \pi$	 π^*

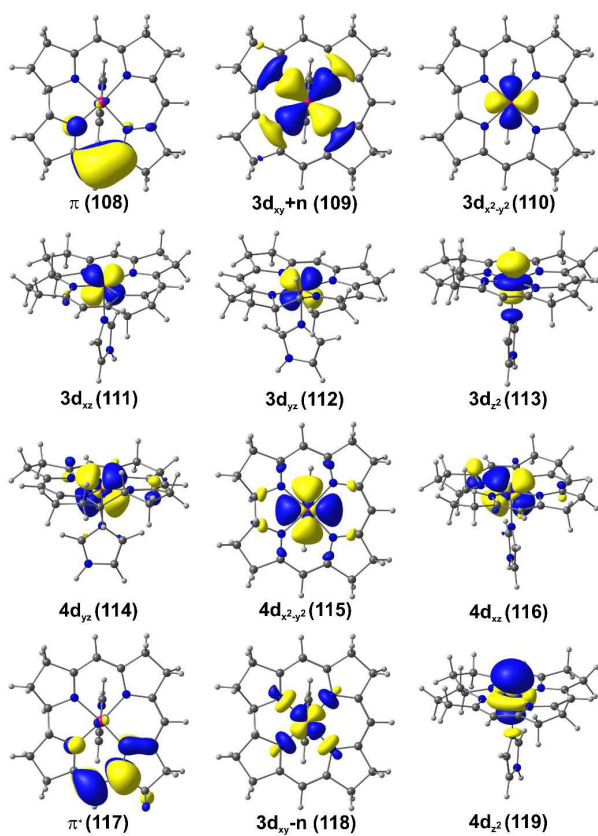


Figure 4. Active orbitals of $\text{Im}[\text{Co}^{\text{II}}(\text{corrin})]^+$ used in the CASSCF(11,12) and subsequent XMCQDPT2 calculations.

Figure 5. NTOs for Im-[Co^{II}(corrin)]⁺ (upper panel) and [Im--Co^{II}(corrin)]⁺, Co-C = 2.80 Å, (lower panel) based on TD-DFT calculations at the uBP86/6-311G(d,p) level.

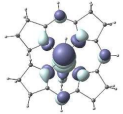
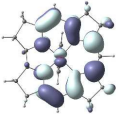
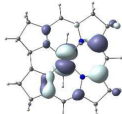
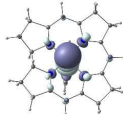
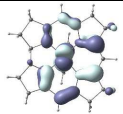
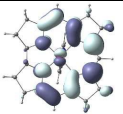
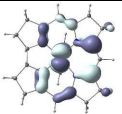
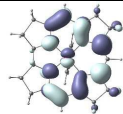
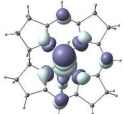
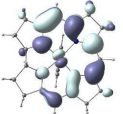
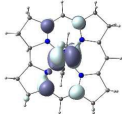
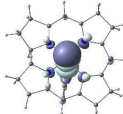
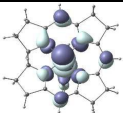
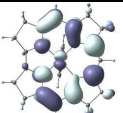
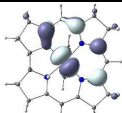
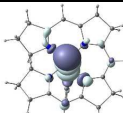
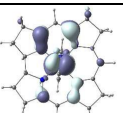
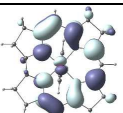
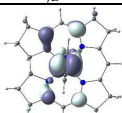
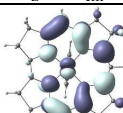
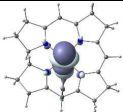
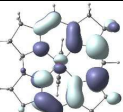
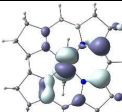
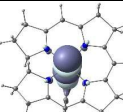
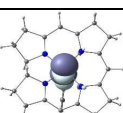
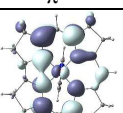
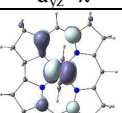
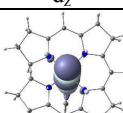
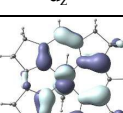
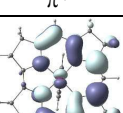
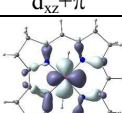
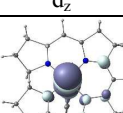
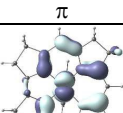
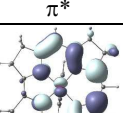
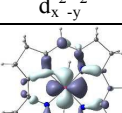
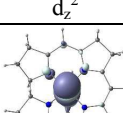
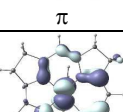
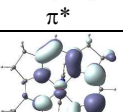
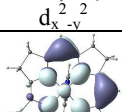
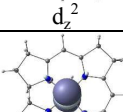
NTO	eV	NTO Coeff	<i>f</i>	α hole	α particle	β hole	β particle
Im-[Co^{II}(corrin)]⁺							
D ₁	1.40	31 (α) 69 (β)	0.0001	 $d_z^2 + \pi_{Im}$	 π^*	 $d_{yz} + \pi$	 $d_z^2 + \pi_{Im}^*$
D ₂	1.50	36 (α) 64 (β)	0.0008	 $d_{yz} + \pi$	 π^*	 $d_{yz} + \pi$	 π^*
D ₃	1.59	16 (α) 83 (β)	0.0010	 $d_z^2 + \pi_{Im}$	 π^*	 $d_{xz} + \pi$	 $d_z^2 + \pi_{Im}^*$
D ₄	1.65	49 (α) 51 (β)	0.0026	 $d_z^2 + \pi_{Im}$	 π^*	 $d_{yz} + \pi$	 $d_z^2 + \pi_{Im}^*$
D ₅	1.81	8 (α) 92 (β)	0.0028	 $d_{xz} + \pi_{Im}$	 π^*	 $d_{xz} + \pi_{Im}$	 π^*
[Im--Co^{II}(corrin)]⁺ (2.80 Å)							
D ₁	0.72	0 (α) 100 (β)	0.000	 d_z^2	 π^*	 $d_{yz} + \pi$	 d_z^2
D ₂	0.91	0 (α) 100 (β)	0.0000	 d_z^2	 π^*	 $d_{xz} + \pi$	 d_z^2
D ₃	1.55	11 (α) 52 (β)	0.0017	 π	 π^*	 $d_x^2 - d_y^2$	 d_z^2
D ₄	1.66	25 (α) 50 (β)	0.0001	 π	 π^*	 $d_x^2 - d_y^2$	 d_z^2
D ₅	1.84	8 (α) 92 (β)	0.0015	 π	 π^*	 π	 d_z^2

Figure 6. Comparison of experimental and simulated spectrum of cob(II)alamin. Experimental cob(II)alamin steady-state spectra (solid line), and TD-DFT transitions of cob(II)alamin at the BP86/SDD level (circles); and of the two truncated structural models with BP86/6-311g(d,p): Im-[Co^{II}(corrin)]⁺, min (filled triangles), and the [Im---Co^{II}(corrin)]⁺ LF state, Co-C = 2.80 Å, (empty triangles). The experimental spectrum was provided by Professor R. J. Sension from University of Michigan, and is also presented in Reference #33.

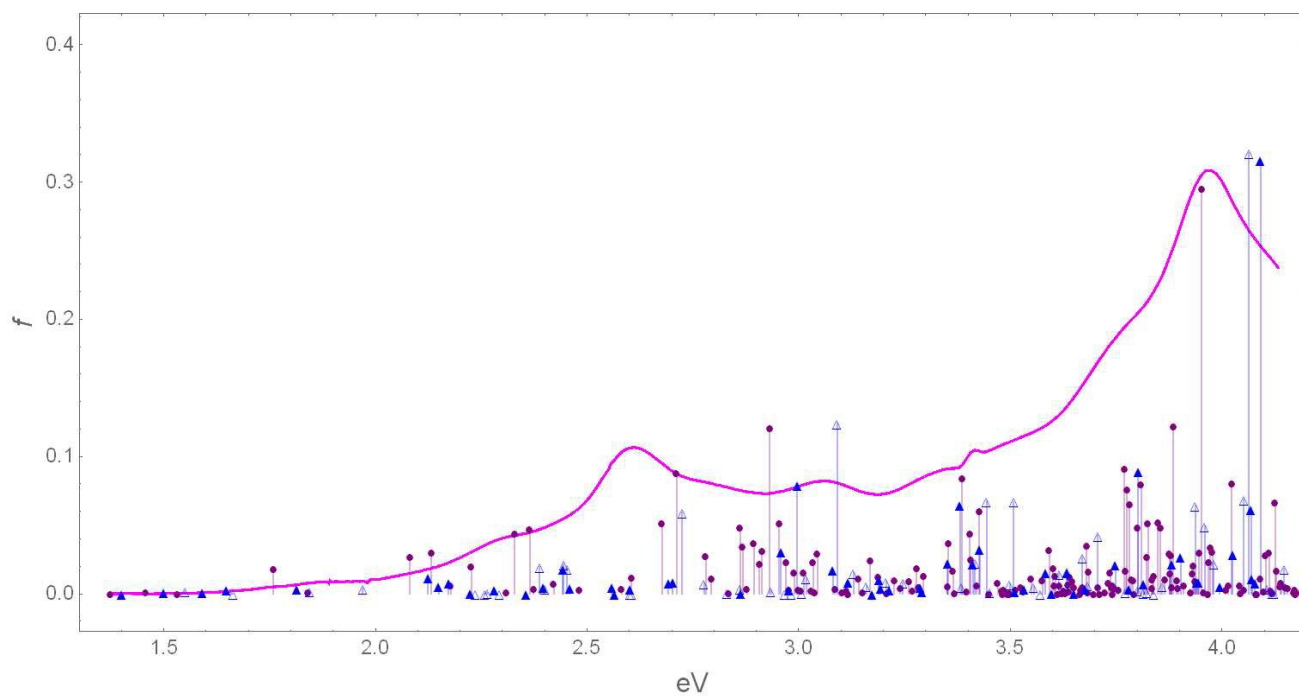
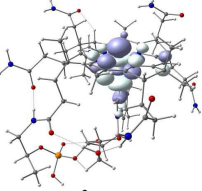
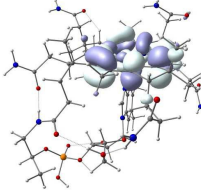
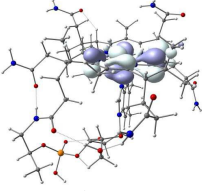
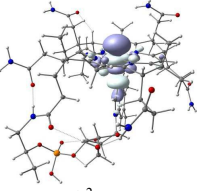
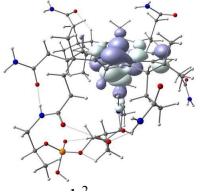
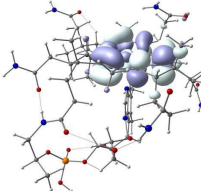
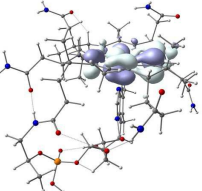
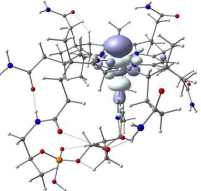
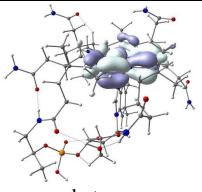
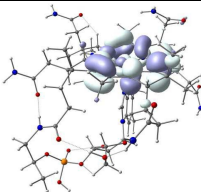
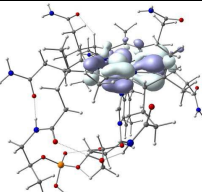
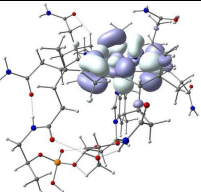
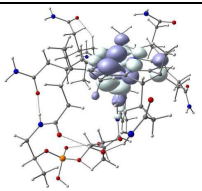
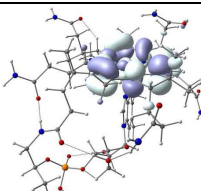
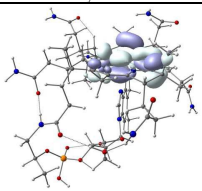
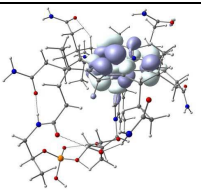
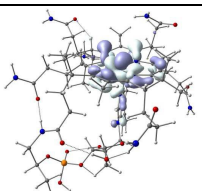
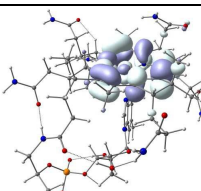
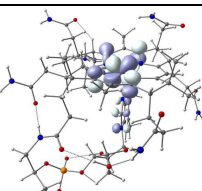
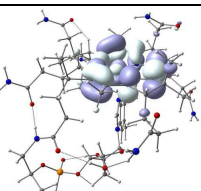


Figure 7. NTOs of the first 5 TDDFT excited states of the cob(II)alamin structure at the BP86/6-311G (d,p) level of theory.

NTO	eV	NTO Coeff	f	α hole	α particle	β hole	β particle
D ₁	1.27	6 (α) 94 (β)	0.0001	 $d_z^2 + \pi_{im}$	 π^*	 $d_{yz} + \pi$	 $d_z^2 + \pi$
D ₂	1.42	0 (α) 100 (β)	0.0001	 $d_z^2 + \pi_{im}$	 π^*	 $d_{xz} + \pi$	 $d_z^2 + \pi$
D ₃	1.48	37 (α) 63 (β)	0.0005	 $d_{yz} + \pi_{im}$	 π^*	 $d_{yz} + \pi$	 π^*
D ₄	1.72	91 (α) 8 (β)	0.0074	 $d_z^2 + \pi_{im}$	 π^*	 $d_{yz} + \pi$	 $d_z^2 + \pi^*$
D ₅	1.78	14 (α) 85 (β)	0.0023	 $d_{xz} + \pi$	 π^*	 $d_{xz} + \pi$	 π^*

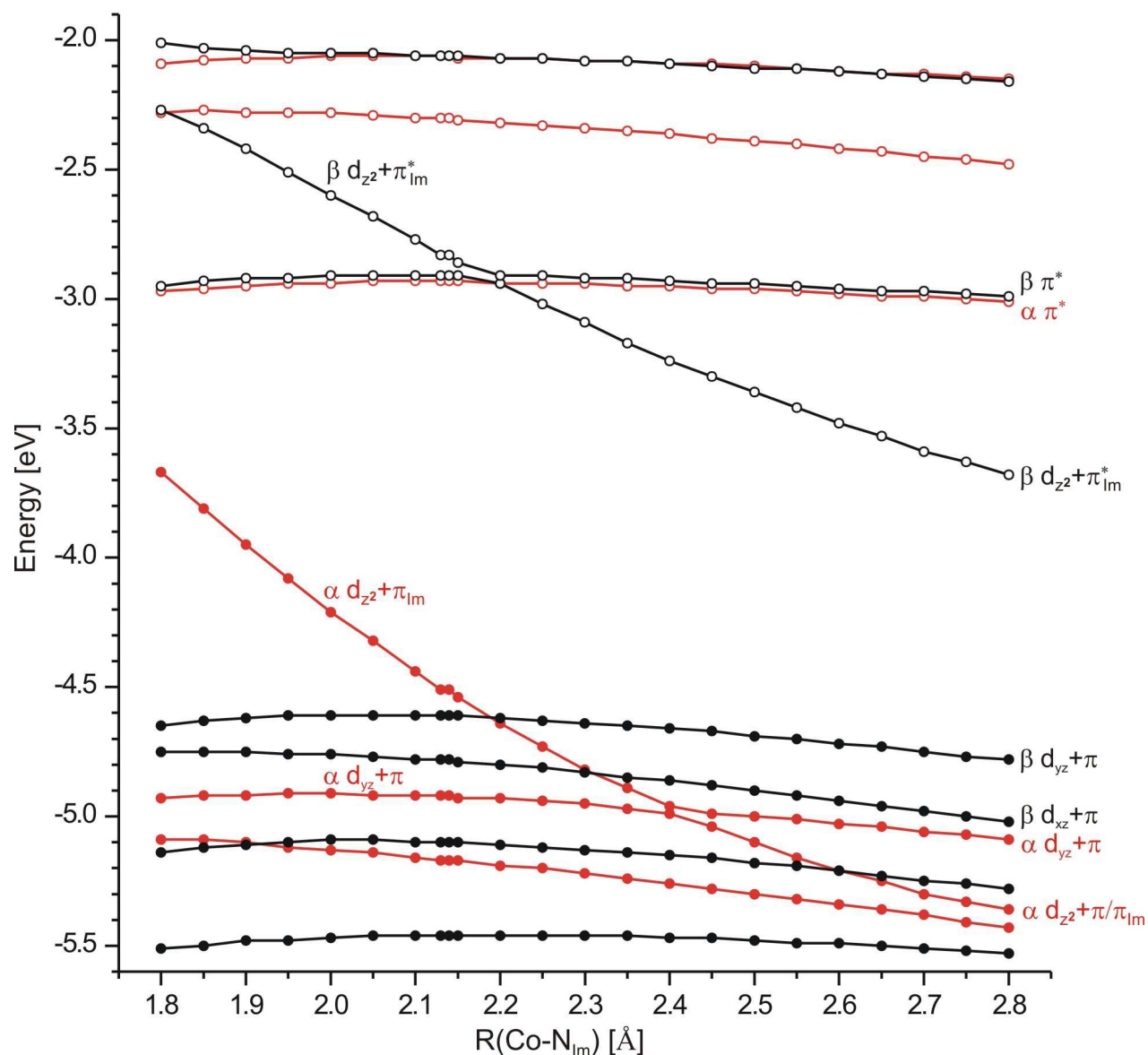


Figure 8. Energies of frontier molecular orbitals for Im-[Co^{II}(corrin)]⁺ model complex as a function of Co-N_{Im} distance. Red line – energies of alpha orbitals, black line – energies of beta orbitals, filled and empty circles correspond to the occupied and unoccupied orbitals, respectively.

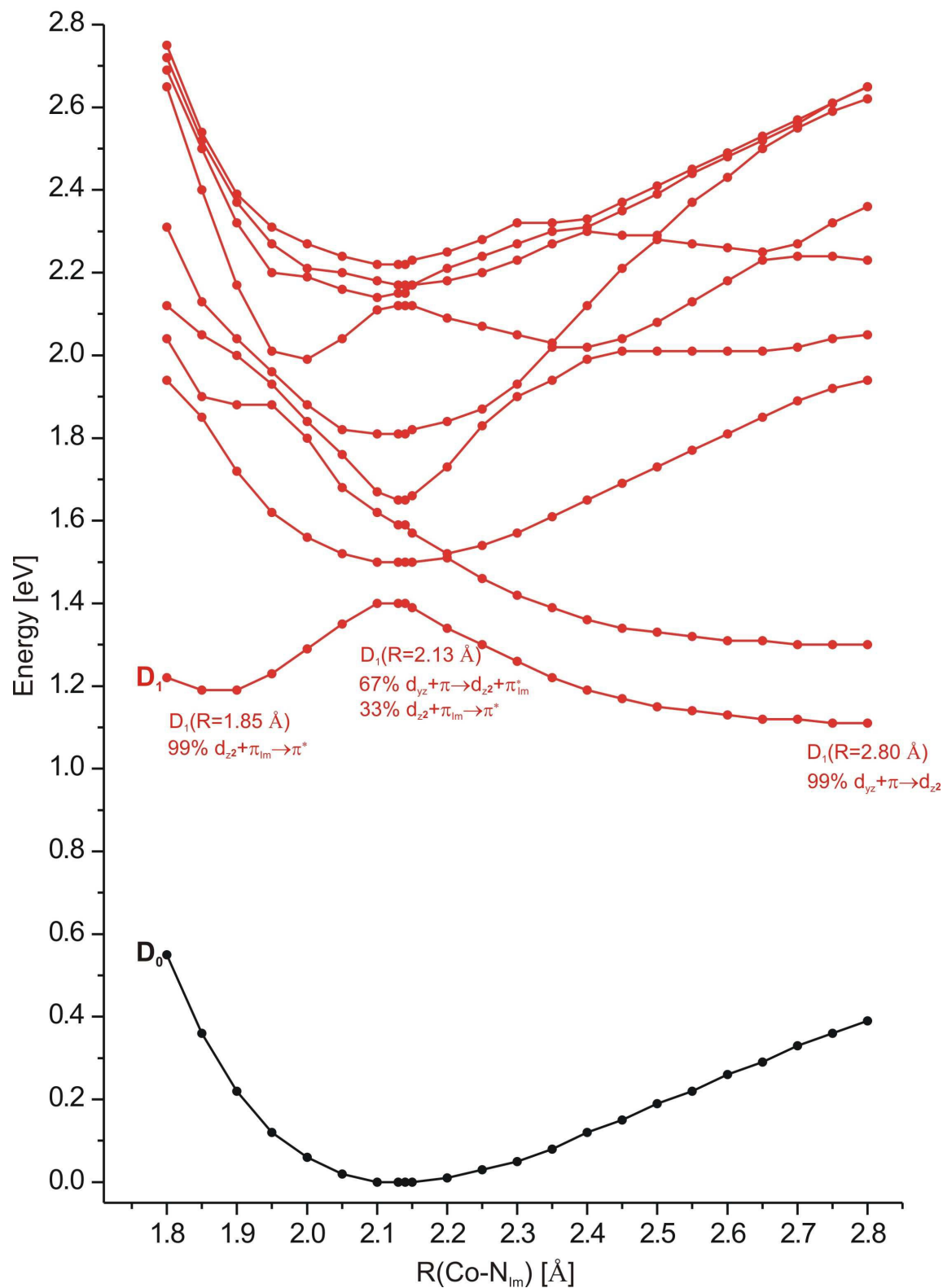


Figure 9. Potential energy curves of the ground and nine lowest doublet TD-DFT excited states of the $\text{Im}[\text{Co}^{\text{II}}(\text{corrin})]^+$ model complex as a function of Co-N_{Im} bond length.